HHS Public Access

Author manuscript

Ann Neurol. Author manuscript; available in PMC 2017 March 21.

Published in final edited form as:

Ann Neurol. 2016 March ; 79(3): 387–403. doi:10.1002/ana.24573.

Reducing Timp3 or Vitronectin Ameliorates Disease Manifestations in CADASIL Mice

Carmen Capone, PhD[1,2], **Emmanuel Cognat, MD**[1,2], **Lamia Ghezali, PhD**[1,2], **Céline Baron-Menguy, PhD**[1,2], **Déborah Aubin, MSc**[1,2], **Laurent Mesnard, MD, PhD**[3,4], **Heidi Stöhr, PhD**[5], **Valérie Domenga-Denier**[1,2], **Mark T. Nelson, PhD**[6,7], and **Anne Joutel, MD, PhD**[1,2]

[1]Genetics and Pathogenesis of Cerebrovascular Diseases, Inserm, U1161 and Univ Paris Diderot, Sorbonne Paris Cité, UMRS 1161, F-75010, Paris, France

[2]DHU NeuroVasc, Sorbonne Paris Cité, Paris, France

[3]Rare and Common Kidney Diseases, Matrix Remodeling and Tissue Repair, Inserm U1155 and Pierre and Marie Curie University, Sorbonne Universities UMR-S 1155, F-75020, Paris, France

[4]Department of Emergency Nephrological and Renal Transplantation, Tenon Hospital, AP-HP, F-75020, Paris, France

[5]Institute of Human Genetics, University of Regensburg, Regensburg, Germany

[6]Department of Pharmacology, College of Medicine, University of Vermont, Burlington, VT

[7]Institute of Cardiovascular Sciences, University of Manchester, Manchester, United Kingdom

Abstract

Objective—CADASIL is a genetic paradigm of cerebral small vessel disease caused by NOTCH3 mutations that stereotypically lead to the extracellular deposition of NOTCH3 ectodomain (Notch3^{ECD}) on the vessels. TIMP3 and vitronectin are 2 extracellular matrix proteins that abnormally accumulate in Notch3^{ECD}-containing deposits on brain vessels of mice and patients with CADASIL. Herein, we investigated whether increased levels of TIMP3 and vitronectin are responsible for aspects of CADASIL disease phenotypes.

Methods—Timp3 and *vitronectin* expression were genetically reduced in *TgNotch3*^{R169C} mice, a well-established preclinical model of CADASIL. A mouse overexpressing human TIMP3 (*TgBAC-TIMP3*) was developed. Disease-related phenotypes, including cerebral blood flow (CBF) deficits, white matter lesions, and Notch3^{ECD} deposition, were evaluated between 6 and 20 months of age.

Address correspondence to Dr Joutel, Faculté de Médecine Paris Diderot, site Villemin, 10 av de Verdun, 75010 Paris, France. anne.joutel@inserm.fr.

Author Contributions

All authors contributed to the design of the study, data analysis, and editing. M.T.N. contributed to drafting the paper. A.J. conceived the study and wrote the manuscript. E.C. and L.G. contributed equally to this work.

Potential Conflicts of Interest

A.J. has a patent “Gene Involved in CADASIL, Method of Diagnosis and Therapeutic Application” licensed to Athena diagnostics, and a patent “Immunological Treatment of CADASIL” pending.

Results—CBF responses to neural activity (functional hyperemia), topical application of vasodilators, and decreases in blood pressure (CBF autoregulation) were similarly reduced in *TgNotch3*^{R169C} and *TgBAC-TIMP3* mice, and myogenic responses of brain arteries were likewise attenuated. These defects were rescued in *TgNotch3*^{R169C} mice by haploinsufficiency of *Timp3*, although the number of white matter lesions was unaffected. In contrast, haploinsufficiency or loss of *vitronectin* in *TgNotch3*^{R169C} mice ameliorated white matter lesions, although CBF responses were unchanged. Amelioration of cerebrovascular reactivity or white matter lesions in these mice was not associated with reduced Notch3^{ECD} deposition in brain vessels.

Interpretation—Elevated levels of TIMP3 and vitronectin, acting downstream of Notch3^{ECD} deposition, play a role in CADASIL, producing divergent influences on early CBF deficits and later white matter lesions.

Cerebral small vessel disease (SVD) accounts for a quarter of ischemic strokes and is increasingly recognized as a leading cause of age- and hypertension-related cognitive decline and disability.[1] CADASIL (cerebral autosomal dominant arteriopathy with subcortical infarcts and leukoencephalopathy), the most common hereditary SVD, is caused by dominant mutations in NOTCH3,[2,3] a heterodimeric receptor that is predominantly expressed in vascular smooth muscle cells and is a critical regulator of the developmental formation of small arteries.[4] CADASIL is characterized by midlife onset of recurrent stroke and cognitive impairment, progressing to dementia and premature death at approximately 60 years of age.[3] Currently, there are no therapies available to prevent or slow the pathogenesis of CADASIL.

CADASIL-associated *NOTCH3* mutations stereotypically lead to the early extracellular deposition of NOTCH3 ectodomain (Notch3^{ECD}) at the plasma membrane of vascular smooth muscle cells and pericytes and in extracellular deposits called granular osmiophilic material (GOM).[5–7] Recently, we and others provided evidence that excess levels or multimerization of mutant Notch3^{ECD} facilitate interactions with key components of the vascular extracellular matrix, including but not limited to TIMP3 and vitronectin, and promote their accumulation in Notch3^{ECD}-containing deposits.[6,8,9]

TIMP3 is a member of the tissue inhibitor of metalloproteinases (TIMP) family, comprising 4 small proteins; as their name implies, these proteins are physiologic inhibitors of metalloproteinases, which degrade the extracellular matrix and promote shedding of cell surface molecules.[10] Vitronectin is an adhesive glycoprotein that coordinates cell adhesion and cell migration with pericellular proteolysis and growth factor signaling.[11] In the normal brain, TIMP3 and vitronectin are predominantly associated with the extracellular matrix of vessels.[6,9]

In this study, we sought to elucidate whether the increase in the levels of TIMP3 and vitronectin extracellular matrix proteins is pathogenic or a mere epiphenomenon.

Material and Methods

Mice

TgNotch3^{R169C} (line 88) and *TgNotch3*^{WT} (line 129) mice, which overexpress mutant and wild-type NOTCH3 receptors, respectively, at comparable levels, were maintained in a heterozygous state on an FVB/N background, as described previously.[12] *Timp3*-null (*Timp3*$^{-/-}$)[13] and *vitronectin*-null (*Vtn*$^{-/-}$) mice[14] on a C57BL/6 background were obtained from B. Weber and H. Stoehr (Regensburg University, Germany) and E. Rondeau (Inserm, France), respectively. FVB/N mice were purchased from Charles River (Charles River Laboratories, Saint-Germain-Nuelles, France). The *TgNotch3*^{R169C}*/Timp3* double-mutant mice used in the study—*TgNotch3*^{R169C}*;Timp3*$^{+/+}$, *TgNotch3*^{R169C}*; Timp3*$^{+/-}$, *non-Tg;Timp3*$^{+/+}$, and *non-Tg;Timp3*$^{+/-}$—were littermates with the same hybrid background (88% FVB/ N:12% C57Bl/6). Likewise, the *TgNotch3*^{R169C}*/Vtn* mice—*TgNotch3*^{R169C}*;Vtn*$^{+/+}$, *TgNotch3*^{R169C}*;Vtn*$^{+/-}$, and *TgNotch 3*^{R169C}*;Vtn*$^{-/-}$, as well as *non-Tg;Vtn*$^{+/+}$, *non-Tg;Vtn*$^{+/-}$, and *non-Tg;Vtn*$^{-/-}$—were littermates on the same hybrid background (81% FVB/N:19% C57Bl/6).

TgBAC-TIMP3 mice were generated using a 182.9kb bacterial artificial chromosome (BAC) clone, hRP11 419C14, containing the entire human *TIMP3* locus. The fidelity of the final product was determined by restriction enzyme fragment mapping, field inversion gel electrophoresis, polymerase chain reaction (PCR), and DNA sequencing. BAC DNA was prepared and purified using the Large-Construct Kit (Qiagen, Valencia, CA) and injected into C57BL/6 mouse oocytes. We established 2 heterozygous transgenic (Tg) lines (lines 2 and 29). The transgene in line 29, which was integrated into chromosome X, was associated with prenatal lethality in males. Hence, line 2 was used for subsequent experimentation. Mice were backcrossed 3 times onto an FVB/N background and maintained on this hybrid background (88% FVB/N: 12% C57Bl/6).

Genotyping analyses were performed by PCR using the following primer pairs: *TgNotch3*, 5′-TCA ACG CCT TCT CGT TCT TC-3′ (forward) and 5′-AAT ACC GTC GTG CTT TCG AG-3′ (reverse); *Timp3* wild-type allele, 5′-TTC AGT AAG ATG CCC CAC G-3′ (forward) and 5′-TAC ATC TTG CCT TCA TAC ACG-3′ (reverse); *Timp3* knockout allele, 5′-TTC AGT AAG ATG CCC CAC G-3′ (forward) and 5′-ATG TGG AAT GTG TGC GAG G-3′ (reverse); *vitronectin* wild-type allele, 5′-TCA GAA GTG TGC CAG TGC TT-3′ (forward) and 5′-GCT GAG CCA TCT TTC CAG TC-3′ (reverse); *vitronectin* knockout allele, 5′-GCC AGA GGC CAC TTG TGT AG-3′ (forward) and 5′-TCA GAA GTG TGC CAG TGC TT-3′ (reverse); and *TgBAC-TIMP3*, 5′-CCA GGA GAC AGC AAG TAG CC-3′ (forward) and 5′-GCT GCT GTT TAG GGA TCT GC-3′ (reverse). Mice were bred and housed in pathogen-free animal facilities (Transgénèse et Archivage d'Animaux Modèles (TAAM) or University Paris 7, site Villemin) and fed a standard diet ad libitum with free access to water. All experiments described in this study were conducted in full accordance with the guidelines of our local institutional animal care and use committee (Lariboisière-Villemin), with every effort made to minimize the number of animals used. Unless otherwise noted, experiments were performed in age-matched littermates to minimize confounding effects attributable to background heterogeneity.

RNA Preparation and Quantitative Reverse Transcription PCR Analyses

RNA was extracted from cerebral pial arteries dissected under a microscope, and quantitative reverse transcription (RT)-PCR was performed as previously described.[15] The following primer pairs were used: murine *Timp3*, 5′-GCC ATT CTC AAT CCC TGG TA-3′ (forward) and 5′-ACC GCT CTC CGA TGA TGT AA-3′ (reverse); murine *vitronectin*, 5′-TGT TTG AGC ACT TTG CCT TG-3′ (forward) and 5′-GTG GGA TAA GGA GCC AGT GA-3′ (reverse); rat *Notch3 transgene*, 5′-CTC CCT GGC TTC TCT CTC-3′ (forward) and 5′-GGT CAG CCC CTA CCC ATT-3′ (reverse); *β-actin*, 5′-CTG CGT CTG GAC CTG GCT-3′ (forward) and 5′-ACG CAC GAT TTC CCT CTC A-3′ (reverse); and *transgelin* 5′-TCT AAT GGC TTT GGG CAG TT-3′ (forward) and 5′-GCA GTT GGC TGT CTG TGA AG-3′ (reverse).

In Vivo Analysis of Cerebrovascular Reactivity

SURGICAL PROCEDURE—Male mice were anesthetized with isoflurane (maintenance, 2%), tracheally intubated, and artificially ventilated with an oxygen–nitrogen mixture using a ventilator (Sar-830/P; CWE, Ardmore, PA). The femoral artery was cannulated for recording mean arterial pressure and collecting blood samples. A small craniotomy (2 × superfused with Ringer solution (37°C; pH 7.3–7.4). After surgery, isoflurane was gradually discontinued and anesthesia was maintained with urethane (750mg/kg^{-1}) and chloralose (50mg/kg^{-1}). Rectal temperature was maintained at 37°C, and arterial blood gases were measured. The level of anesthesia was monitored by testing corneal reflexes and motor responses to tail pinch. To minimize confounding effects of anesthesia on vascular reactivity, we kept the time interval between the administration of urethane–chloralose and the testing of cerebral blood flow (CBF) responses consistent among the different groups of mice studied. Arterial blood pressure, blood gases, and rectal temperature were monitored and controlled (Table).

CBF MONITORING—Relative CBF was continuously monitored at the site of the cranial window using a laser-Doppler probe (Moor Instruments, Axminster, UK) positioned stereotaxically 0.5 to 1mm from the cortical surface. CBF values were expressed as percentage increase relative to the resting level ($[CBF_{stimulus} - CBF_{resting}]/CBF_{resting}$). Zero values for CBF were obtained after the heart was stopped by an overdose of isoflurane at the end of the experiment.[16] Laser-Doppler flowmetry provides an accurate assessment of relative CBF changes, but it does not provide measurements of absolute flow.

CBF recordings were started after arterial pressure and blood gases had reached a steady state, as previously described.[16] All pharmacological agents studied were dissolved in a modified Ringer solution.[17] The increase in CBF produced by somatosensory activation was studied by stimulating the whiskers contralateral to the cranial window by side-to-side deflection for 60 seconds. Acetylcholine (10 μmol/l; Sigma-Aldrich, St Louis, MO) or the calcium ionophore A23187 (3 μmol/l; Sigma-Aldrich), both endothelium-dependent vasodilators, were topically superfused for 5 minutes, and the resulting changes in CBF were monitored. CBF responses to the smooth muscle–dependent relaxant adenosine (400 μmol/l; Sigma-Aldrich) were also examined. The lower limit of CBF autoregulation was determined at the end of the experiment, as previously described.[18] Considering that basal cortical blood

flow in *TgNotch3*^{R169C} mice is weakly reduced (by 5–8% at 12 months of age),[12] the amplitude of evoked CBF responses is unlikely to be affected by a ceiling effect.

Ex vivo Analysis of Myogenic Tone

Myogenic responses were analyzed on segments of the posterior cerebral artery, and myogenic tone was determined by increasing intraluminal pressure from 10 to 100mmHg using a pressure-servo control pump as previously described.[12] Myogenic tone was expressed as the percentage of passive diameter ([passive diameter − active diameter]/ passive diameter × 100).

Immunoblot Analysis

Protein extracts were prepared from cerebral pial arteries and subjected to immunoblotting using rabbit monoclonal anti–TIMP-3 (1:2,500, clone D74B10; Cell Signaling Technology, Danvers, MA), and mouse monoclonal anti–smooth muscle alpha actin (1:25,000, clone 1A4, Sigma-Aldrich) as previously described.[6] Densitometric quantification of band intensity was performed using ImageJ (v10.2, NIH).

Immunohistochemistry

For myelin basic protein (MBP) staining, mice were deeply anesthetized with sodium pentobarbital (80mg/kg) and transcardially perfused with 50ml of phosphate buffer (PB) followed by 50ml of 4% paraformaldehyde in PB. The brain was removed, postfixed in 4% paraformaldehyde, and processed for cryopreservation. Free-floating cryosections (16 μm-thick sagittal slices, n = 4–8 sections/mouse) were immunostained with mouse monoclonal anti-MBP antibody (1:10,000, SMI94; BioLegend, London, UK) as described.[19]

For Notch3^{ECD} staining, mice were overdosed with isoflurane, and brains were harvested, frozen in liquid nitrogen, and stored at −80°C. Acetone-fixed cryosections (12 μm thick, n = 9 sections/mouse) were incubated overnight at 4°C with rabbit polyclonal anti-Notch3^{ECD} primary antibody raised against epidermal growth factor repeats 17 to 21 of rat Notch3 (1:16,000; A.J., unpublished data), followed by detection with Alexa 594-conjugated antirabbit secondary antibody (1:500; Life Technologies, Saint Aubin, France). Arteries were identified by immunostaining with fluorescein isothiocyanate–conjugated anti–smooth muscle α-actin primary antibody (1:1,000, clone 1A4, Sigma-Aldrich), and capillaries were identified by immunostaining with rat monoclonal antiperlecan antibody (1:500, clone A7L6; Millipore, Molsheim, France) followed by detection with Alexa 488–conjugated antirat secondary antibody (1:500; Life Technologies).

Quantification of Myelin Debris and Notch3^{ECD} Deposits

Stained sections were imaged with an Eclipse 80i microscope (Nikon, Champigny sur Marne, France) at × 20 (MBP analysis), × 40 (capillary analysis), or × 60 (artery analysis) magnification. Images were captured using an Andor Neo sCMOS camera and NIS Elements BR v4.0 software (Nikon), with identical settings across compared groups. The entire procedure was performed with prefixed parameters under blinded conditions.

Myelin debris spots were counted over the whole corpus callosum using a custom-made, 3-step NIH ImageJ macro, as described.[19] Results were expressed as the number of SMI94 hyperintense foci over the area of the corpus callosum.

Notch3^{ECD} deposits were counted on maximal intensity projections of image stacks using ImageJ software (v1.49g; Fiji Distribution, NIH) following a semiautomated procedure that includes 3 main steps: (1) manual delineation of pial arteries on the smooth muscle α-actin channel and delineation of capillaries by automated segmentation on the perlecan channel, followed by measurement of vessel area; (2) background suppression on the Notch3^{ECD} channel; and (3) automatic detection and counting of Notch3^{ECD} deposits within vessel borders using a local maxima approach. Results were expressed as the number of Notch3^{ECD} deposits over the vessel area.

Analysis and Quantification of GOM Deposits

Ultrathin sections of brain artery were prepared and observed in a CM100 electron microscope (Philips, Best, the Netherlands), as previously described.[12] Electron micrograph images of the artery over its entire circumference were captured using a digital camera at ×9,700 magnification. The number of GOM deposits on the abluminal perimeter of smooth muscle cells was counted in a blinded manner. Results were expressed as the number of GOM deposits per 100 μm.

Statistics

Data are expressed as mean ± standard error of the mean. CBF autoregulation and myogenic tone were analyzed by 2-way repeated-measure analysis of variance (ANOVA) followed by Bonferroni post hoc test. Myelin debris, CBF responses, Notch3^{ECD} aggregates, and GOM deposits were analyzed by 1-way ANOVA followed by Bonferroni or Tukey post hoc tests, with the exception of GOM deposits in part C of the last figure, which were analyzed using Student *t* test. Differences with *p*-values < 0.05 were considered statistically significant.

Results

Genetic Reduction of *Timp3* or *Vitronectin* in the *TgNotch3^{R169C}* Mouse Model

To investigate the potential role of TIMP3 and vitronectin in CADASIL pathogenesis, we adopted a genetic interaction approach using the *TgNotch3^{R169C}* mouse model, a well-established preclinical model of CADASIL.[12] Mice completely lacking TIMP3 exhibit various developmental defects, including vascular alterations such as dilated vessels in the eye and outward remodeling of the mesenteric arteries, as well as decreased arterial blood pressure.[13,20,21] To avoid potentially confounding developmental effects induced by the loss of TIMP3, we generated and analyzed *TgNotch3^{R169C}* mice lacking 1 allele of *Timp3* (*TgNotch3^{R169C};Timp3$^{+/-}$*) along with their control littermates. *Vitronectin*-null mice (*Vtn$^{-/-}$*) show no overt phenotype if unchallenged.[14] Hence, we generated and analyzed *TgNotch3^{R169C}* mice lacking 1 (*TgNotch3^{R169C};Vtn$^{+/-}$*) or 2 (*TgNotch3^{R169C};Vtn$^{-/-}$*) alleles of *vitronectin* along with their control non-Tg littermates. Double-Tg mice were born at the expected Mendelian ratio, and were indistinguishable from the wild-type and *TgNotch3^{R169C}* littermates, even with aging, suggesting a lack of overt deficits. We

confirmed reduction of *Timp3* and *vitronectin* mRNA expression in brain arteries by quantitative RT-PCR analysis of dissected vessels (Fig 1A, C). Notably, *Timp3* mRNA reduction in *Timp3*$^{+/-}$ mice was likely underestimated, as mRNA decay is incomplete in this *Timp3*$^{-/-}$ line (A.J., unpublished data). Importantly, genetic reduction of *Timp3* (*Timp3*$^{+/-}$) or *vitronectin* (*Vtn*$^{+/-}$, *Vtn*$^{-/-}$) in *TgNotch3*^{R169C} mice did not affect *Notch3* transgene mRNA expression compared to their *TgNotch3*^{R169C} littermates on a wild-type *Timp3* (*Timp3*$^{+/+}$) and *vitronectin* (*Vtn*$^{+/+}$) background, respectively (see Fig 1B, D). Therefore, any phenotypic change in these double-mutant mice cannot be attributed to an alteration in *Notch3* transgene expression.

TgNotch3^{R169C} Mice Exhibit a Profound Global Vasomotor Dysfunction That Is Rescued by Genetic Reduction of *Timp3*, but Not *Vitronectin*

We first sought to elucidate the effects of excess TIMP3 and vitronectin on cerebrovascular dysfunction elicited by R169C mutant NOTCH3. We previously reported that functional hyperemia—the process that serves to match local CBF with metabolic demands imposed by neuronal activity in the brain[22]—was disrupted in *TgNotch3*^{R169C} mice as early as 6 months; also the lower limit of CBF autoregulation was significantly shifted to higher blood pressure, reflecting an inability of cerebral vessels to dilate in response to a decrease in arterial blood pressure.[12] Using laser-Doppler flowmetry in mice equipped with an open cranial window over the somatosensory cortex, we monitored CBF increases to whisker stimulation (functional hyperemia) and CBF changes to stepwise reduction of arterial blood pressure (lower limit of CBF autoregulation) in a cohort of 6-month-old double-Tg mice and appropriate age-matched controls. As expected, we observed compromised functional hyperemia and autoregulation in *TgNotch3*^{R169C} mice (Fig 2). These defects were retained in *TgNotch3*^{R169C}*;Timp3*$^{+/+}$ and *TgNotch3*^{R169C}*; Vtn*$^{+/+}$ mice with wild-type *Timp3* and *vitronectin* alleles, obtained by crossing *TgNotch3*^{R169C} mice with the corresponding heterozygous mice, indicating that minor differences in strain background between genotypes did not affect the *TgNotch3*^{R169C} phenotype. Importantly, genetic reduction of *Timp3* (*TgNotch3*^{R169C}*;Timp3*$^{+/-}$) restored functional hyperemia and the lower limit of autoregulation. In contrast, these deficits were unaffected by genetic reduction (*TgNotch3*^{R169C}*;Vtn*$^{+/-}$) or elimination (*TgNotch3*^{R169C}*; Vtn*$^{-/-}$) of *vitronectin*.

To explore the extent to which the rescue of the mutant NOTCH3 functional phenotype can be generalized, we assessed CBF responses to endothelial-dependent and smooth muscle–dependent vasodilators applied to the cranial window. The increase in CBF evoked by topical application of the endothelium-dependent vasodilators acetylcholine or A23187 (Ca^{2+} ionophore) was significantly reduced in *TgNotch3*^{R169C} mice compared with *TgNotch3*^{WT} and non-Tg littermates; CBF responses to the smooth muscle relaxant adenosine were likewise significantly reduced in *TgNotch3*^{R169C} mice (Fig 3). Again, as expected, these cerebrovascular responses were similarly impaired in *TgNotch3*^{R169C}*;Timp3*$^{+/+}$ and *TgNotch3*^{R169C}*; Vtn*$^{+/+}$ mice. As was the case for hyperemic responses, CBF responses to vasodilators were not improved in *TgNotch3*^{R169C}*;Vtn*$^{+/-}$ or *TgNotch3*^{R169C}*;Vtn*$^{-/-}$ mice with a reduction or elimination of *vitronectin*. In striking contrast, these responses were completely normal in *TgNotch3*^{R169C}*;Timp3*$^{+/-}$ mice, with reduced expression of *Timp3*. Collectively, these data suggest that *TgNotch3*^{R169C} mice

exhibit a global cerebrovascular dysfunction with a profound reduction in vasodilatory responses, and that decreasing levels of *Timp3*, but not *vitronectin*, protects *TgNotch3*^{R169C} mice from this dysfunction.

Genetic Reduction of *Timp3* Rescues Myogenic Responses in *TgNotch3*^{R169C} Mice

We next asked whether the protection provided by decreasing the amount of *Timp3* acts at the level of brain vessels, as suggested by the predominant vascular expression pattern of TIMP3 in the brain.[6] We previously reported that pressure-induced constriction (myogenic tone) of both pial and parenchymal arteries was markedly attenuated in *TgNotch3*^{R169C} mice.[12,23] Myogenic tone establishes the basal constriction of an artery, providing a state from which an artery can increase or decrease in diameter on demand. A decrease in the myogenic tone of cerebral arteries in *TgNotch3*^{R169C} mice implies a diminution in the vasodilatory reserve that logically could represent a common mechanism for the global cerebrovascular dysfunction exhibited by these mice.[24] To explore the contribution of *Timp3* to this defect, we measured changes in diameter in response to changes in intraluminal pressure in pial arteries from *TgNotch3*^{R169C} mice with normal or reduced expression of *Timp3* at 6 months of age. Reducing *Timp3* had no effect on the myogenic tone in arterial segments from non-Tg mice (*non-Tg;Timp3*$^{+/-}$), but normalized myogenic tone in arteries from *TgNotch3*^{R169C} mice (*TgNotch3*^{R169}*;Timp3*$^{+/-}$; Fig 4A). Hence, our findings suggest that excess TIMP3 acts at least at the level of isolated brain arteries to impair myogenic responses in *TgNotch3*^{R169C} mice.

Genetic Overexpression of TIMP3 Mimics the Cerebrovascular Dysfunction Produced by Mutated *Notch3* in *TgNotch3*^{R169C} Mice

To further investigate the contribution of TIMP3 to cerebrovascular dysfunction, we tested whether elevated TIMP3 expression reproduced the cerebrovascular deficits of *TgNotch3*^{R169C} mice. To this end, we developed a mouse overexpressing human TIMP3 using the endogenous human promoter on a BAC containing the human genomic *TIMP3* locus. The full-length *TIMP3* transcription unit is nested within intron V of the *synpasin 3* gene, and with the exception of exons 5 to 7 of this gene, no other known or predicted genes lie on this BAC (see Fig 4B). Immunoblot analyses of pial arteries revealed that TIMP3 expression was increased ~4-fold over the endogenous murine TIMP3 in *TgBAC-TIMP3* mice (see Fig 4C, D).

Remarkably, CBF responses to functional hyperemia, topical application of vasodilators, and decreases in blood pressure were similarly reduced in *TgBAC-TIMP3* and *TgNotch3*^{R169C} mice (see Figs (2 and 3), and 4E–I). Likewise, myogenic responses of brain arteries were attenuated in *TgBAC-TIMP3* mice (see Fig 4J). Taken together, our findings indicate that elevated TIMP3 expression is responsible for the global impairment of cerebral vasodilatory responses and the attenuation of myogenic responses of brain arteries.

Reducing the Gene Dosage of *Vitronectin*, but Not *Timp3*, Ameliorates White Matter Lesions in *TgNotch3*^{R169C} Mice

We next evaluated the impact of reducing *Timp3 or vitronectin* gene dosage on white matter lesions elicited by mutant NOTCH3. We previously reported that *TgNotch3*^{R169C} mice

develop vacuolation of the cerebral white matter tracts around the age of 20 months.[12] Subsequent analyses revealed that white matter vacuolation was associated with segmental degradation of myelin fibers, as evidenced by immunolabeling brain sections with the SMI94 anti-MBP antibody. Notably, an assessment of the number of fluorescent foci (myelin debris) proved to reflect white matter pathology more accurately—and earlier—than vacuolation.[19] Accordingly, we used SMI94 brain immunostaining to characterize a cohort of double-mutant mice and appropriate controls at 6, 12, and 20 months of age. *TgNotch3*^{R169C} mice on a wild-type *vitronectin* or *Timp3* background exhibited a significantly higher number of myelin debris spots at 6 months of age compared with age-matched wild-type non-Tg littermates. The number of these lesions almost doubled between 6 and 12 months and between 12 and 20 months of age (Figs 5 and 6). Importantly, genetic reduction of *Timp3* (*TgNotch3*^{R169C};*Timp3*$^{+/-}$) had no effect on white matter lesions at 6, 12, or 20 months of age (see Fig 5). In striking contrast, the severity of white matter lesions was significantly attenuated by genetic reduction of *vitronectin* (*TgNotch3*^{R169C};*Vtn*$^{+/-}$) at 12 and 20 months of age (see Fig 6). Moreover, mutant mice lacking *vitronectin* (*TgNotch3*^{R169C};*Vtn*$^{-/-}$) exhibited a significantly lower number of myelin debris spots at 20 months of age. Consistent with the observation that expression of vitronectin in *TgNotch3*^{R169C} mice is altered at or above the age of 12 months,[6] genetic reduction or elimination of *vitronectin* had no detectable effect on the number of myelin debris at 6 months of age. Thus, these data suggest that increased levels of vitronectin alone, but not TIMP3 alone, contribute to CADASIL-related white matter lesions.

The above results show that reducing the gene dosage of *vitronectin* does not rescue the cerebrovascular dysfunction at 6 months of age but ameliorates the white matter lesions at 12 months of age. To further investigate the possibility that amelioration of white matter lesions occurs without restoration of CBF deficits, we assessed CBF responses at 12 months of age in *TgNotch3*^{R169C} mice with normal (*TgNotch3*^{R169C};*Vtn*$^{+/+}$) or half reduced expression (*TgNotch3*^{R169C};*Vtn*$^{+/-}$) of vitronectin and appropriate controls. We found that the increases in CBF evoked by whisker stimulation, endothelium-dependent vasodilators, and adenosine as well as the lower limit of the autoregulation were similarly impaired in *TgNotch3*^{R169C};*Vtn*$^{+/+}$ and *TgNotch3*^{R169C};*Vtn*$^{+/-}$ mice (data not shown). Collectively, these data support the conclusion that, in *TgNotch3*^{R169C} mice, white matter pathology can develop in the presence of normal cerebrovascular reactivity and that phenotypic rescue of these lesions can occur without rescue of cerebrovascular deficits.

Vascular Notch3^{ECD} Deposition is Unaffected by Genetic Reduction of *Timp3* or *Vitronectin*

Our working hypothesis is that multimerization and extracellular deposition of mutant Notch3^{ECD} leads to accumulation of TIMP3 and vitronectin. The present data suggest that both of these proteins exert biological effects. It is also possible that the mutant Notch3^{ECD} is directly involved in the pathology, and that TIMP3 and/or vitronectin are involved in the development of Notch3^{ECD} deposits. To test this possibility, we used quantitative immunofluorescence and transmission electron microscopy to assess the burden of Notch3^{ECD} and GOM deposits in the brain vessels of double mutants. We analyzed *TgNotch3*^{R169C} mice with normal or reduced expression of *Timp3* at 6 months of age as we did in the rescue experiments (see Figs 2 and 3). We conducted similar analyses in

TgNotch3^{R169C} mice with normal, reduced, or no expression of *vitronectin* at 12 months of age (see Fig 6). The number of Notch3^{ECD} deposits in arteries and capillaries was unaffected by reduction of *Timp3* (Fig 7). From 6 to 12 months of age, the number of Notch3^{ECD} deposits in brain arteries and capillaries from *TgNotch3*^{R169C} mice on a wild-type background increased by 40 to 50%. Importantly, genetic reduction or elimination of *vitronectin* did not affect the number of Notch3^{ECD} deposits in brain vessels. Similarly, the number of GOM deposits in brain arteries was unaffected by genetic reduction of *Timp3* or *vitronectin* (Fig 8). Collectively, these data indicate that the protection provided by decreasing levels of *Timp3* or *vitronectin* in *TgNotch3*^{R169C} mice does not involve reduced deposition of Notch3^{ECD}, supporting the idea that Notch3^{ECD} deposition is upstream of the accumulation of TIMP3 and vitronectin.

Discussion

Recently, we proposed the possibility that excess levels of extracellular matrix proteins, like TIMP3 or vitronectin, which are abnormally recruited in Notch3^{ECD}-containing deposits, might contribute to the pathogenesis of CADASIL.[6] In the present study, we tested this hypothesis using genetic-interaction approaches in a well-established preclinical mouse model of CADASIL. Our results provide genetic evidence that excess levels of TIMP3 and vitronectin contribute to 2 important pathophysiological events— compromised cerebrovascular reactivity and white matter lesions—and that Notch3^{ECD} deposition is at the top of the pathogenic cascade. Although we cannot exclude interactive effects of increased TIMP3 and vitronectin, our results support the concept of divergent influences on early deficits in the control of CBF (TIMP3) and later increases in white matter lesions (vitronectin). The pathological weight of accumulated TIMP3 and vitronectin on cognitive decline and stroke remains to be determined; a major obstacle is the lack of a suitable model.[25]

Our work provides proof-of-concept that proteins detected in Notch3^{ECD}-containing deposits play a pathophysiological role in CADASIL. The finding that white matter lesions are only partially rescued by manipulating vitronectin expression level suggests that other proteins might be in play. The protein content of Notch3^{ECD}-containing deposits in brain vessels from mice or patients with CADASIL is as yet only partly understood.[6,8,9,26] Thus, our study supports further investigation of these proteins, especially at the early stage of the disease.

An intriguing observation in CADASIL is that, despite the widespread distribution of Notch3^{ECD} deposition in both the cerebral and peripheral vasculature, the clinical manifestations are essentially restricted to the brain.[3] Our work suggests the attractive hypothesis that elevated levels of the proteins that contribute to the pathogenesis might be restricted to the cerebrovasculature. Interestingly, our preliminary analysis revealed that vitronectin, which is robustly expressed in the brain capillaries, is almost undetectable in capillaries of the heart or the kidney, organs commonly spared in CADASIL.

We found that reducing the gene dosage of *Timp3* or *vitronectin* did not aggravate disease manifestations, but instead ameliorated them. The simplest interpretation of these results is

that excess TIMP3 and vitronectin contribute to the disease through an increase in their biological activity. This interpretation is seemingly at odds with the dominant view that proteins trapped in aggregates lose their biological activity.[27] However, there are several possible explanations, at least for TIMP3, for these apparently counterintuitive results. First, our previous biochemical studies revealed that not only insoluble cross-linked TIMP3 species but also soluble TIMP3 species accumulate in the brain vessels of *TgNotch3*^{R169C} mice and patients with CADASIL, although the exact mechanism by which these soluble species accumulate is not entirely clear. Consistent with the observed accumulation of soluble species, reverse zymography analyses have provided evidence for elevated TIMP3 activity in these vessels.[6] Thus, taken together with the mouse genetic results, these biochemical data are consistent with a pathological increase in TIMP3 biological activity. Second, TIMP3 might be sequestrated in Notch3^{ECD}-containing deposits with 1 or more of its substrates. Given that TIMP3 acts as an inhibitor of proteases, a gain in TIMP3 activity in such a scenario could manifest as a loss in the activity of TIMP3 substrates. Third, it has been documented that proteins can dynamically or reversibly associate with aggregates, implying the availability of a pool of unassociated, active proteins.[28] An alternative interpretation of our results is that elevated levels of TIMP3 or vitronectin might contribute to the disease through a toxic gain of function. For instance, TIMP3 or vitronectin might be sequestrated away from their normal subcellular location and gain novel biological activities.

Although we cannot formally exclude changes in other cellular components of the neurovascular unit,[29] the global vasomotor dysfunction observed in *TgNotch3*^{R169C} mice suggests a primary alteration in the vasomotor apparatus, namely vascular smooth muscle cells[30,31]; our data further suggest that excess TIMP3 is a critical contributor to this dysfunction. Several lines of evidence support this interpretation. First, vascular smooth muscle cells are the main source of NOTCH3 in the normal brain, and in patients and mice with CADASIL, and Notch3^{ECD} accumulates at the plasma membrane and in the immediate vicinity of these cells.[5,12] Second, myogenic responses of isolated brain arteries are strongly attenuated in *TgNotch3*^{R169C} mice, and this defect is rescued by reducing expression of *Timp3*. Third, decreased myogenic responses are expected to decrease vasodilatory reserve and thus impair cerebral vasodilatory responses.[24] Accordingly, *TgNotch3*^{R169C} mice exhibit profoundly reduced vasodilation in response to diverse stimuli; importantly, reducing expression of *Timp3* normalizes all these CBF responses and increasing TIMP3 expression reproduces these deficits.

Recent work provides insight into the potential mechanism by which increased TIMP3 activity might impair arterial tone and cerebrovascular function. Specifically, Dabertrand et al demonstrated that the diminished myogenic response in *TgNotch3*^{R169C} mice is caused by an increase in the number of voltage-gated potassium (K_V) channels in smooth muscle cells, and further showed that this defect could be rescued by promoting epidermal growth factor receptor (EGFR)-mediated K_V channel endocytosis using the EGFR agonist heparin-binding epidermal growth factor (HB-EGF).[23] Accordingly, increased levels of TIMP3, which inhibits metalloproteases, could lead to decreased shedding of HB-EGF,[32] and thereby could lead to the suppression of HB-EGF–mediated K_V channel endocytosis and thus an increase in K_V channels in the plasma membrane.

Our study shows that reducing the levels of vitronectin dramatically attenuated the severity of white matter lesions in *TgNotch3*^{R169C} model mice. Notably, this phenotypic rescue occurred without overt restoration of evoked CBF responses. These results raise 2 important questions. First, what are the precise mechanisms underlying the development of white matter injury in this CADASIL model? At first blush, our data suggest that dysregulation of CBF does not participate in the development of white matter injury, a finding that would fly in the face of conventional wisdom.[33] Nonetheless, our prior and present data provide support for this interpretation. White matter lesions in *TgNotch3*^{R169C} mice develop as early as 6 months, whereas resting blood flow in the white matter, as measured by quantitative autoradiography, is not significantly reduced until the age of 20 months.[12] Moreover, restoration of evoked CBF responses by genetic reduction of *Timp3* at 6 months of age is not associated with an attenuation of white matter lesion number. However, we recognize that additional long-term studies are needed to evaluate the CBF deficits and the benefit of reducing *Timp3* expression with age. Moreover, it might also be worthwhile to assess resting flow in the hemispheric white matter in “rescued mice” at 20 months of age. It should also be stressed that the *TgNotch3*^{R169C} mouse model might not recapitulate the full spectrum of white matter lesions encountered in CADASIL. Thus, future studies should seek to investigate other mechanisms that have been proposed to lead to white matter injury in cerebral SVD.[33] Among these, alterations in the permeability of the blood–brain barrier within the hemispheric white matter are not supported by our previous structural and functional analyses of the *TgNotch3*^{R169C} model.[12,19] A second important, as yet unresolved, question is how vitronectin contributes to white matter pathology. In the brain, vitronectin is predominantly expressed in the vasculature,[6] particularly in the capillaries (data not shown). Interestingly, both microarray analyses of purified vascular cells[34] and RNA sequencing of different brain cell populations[35] have shown that vitronectin is enriched in brain pericytes, a finding that is highly consistent with our immunohistochemical analysis (data not shown). The contribution of vitronectin, as well as the potential involvement of pericytes, in white matter pathology deserves further investigation.

In summary, our study identifies a new early stage disease mechanism in CADASIL—accumulation of TIMP3 and vitronectin—that provides a first missing link between Notch3^{ECD} deposition and disease manifestations. Our work suggests that the optimal therapeutic strategy may require targeting Notch3^{ECD} proteins, either by reducing their synthesis, by promoting their clearance, or by preventing the subsequent recruitment of these extracellular matrix proteins.

Acknowledgments

This work was supported by grants from the National Research Agency, France (ANR Genopath 2009-RAE09011HSA, ANR Blanc 2010-RPV11011HHA, A.J.), NIH (NIDDK R37DK053832, NHLBI -P01HL095488, NHLBI R01HL121706, M.T.N.), Totman Medical Research Trust (M.T.N.), and Leducq Foundation (Transatlantic Network of Excellence on the Pathogenesis of SVD of the Brain; A.J., M.T.N.). E.C. is a recipient of fellowships from Inserm (Poste Accueil).

We thank M. Monet-Leprêtre and S. Cleophax for excellent technical assistance, C. Diaz and J. P. Rio for providing assistance with electron microscopy, and TAAM-Orleans and Paris Diderot University–site Villemin for animal housing.

References

1. Pantoni L. Cerebral small vessel disease: from pathogenesis and clinical characteristics to therapeutic challenges. Lancet Neurol. 2010; 9:689–701. [PubMed: 20610345]
2. Joutel A, Corpechot C, Ducros A, et al. Notch3 mutations in CADASIL, a hereditary adult-onset condition causing stroke and dementia. Nature. 1996; 383:707–710. [PubMed: 8878478]
3. Chabriat H, Joutel A, Dichgans M, et al. Cadasil. Lancet Neurol. 2009; 8:643–653. [PubMed: 19539236]
4. Fouillade C, Monet-Leprêtre M, Baron-Menguy C, Joutel A. Notch signalling in smooth muscle cells during development and disease. Cardiovasc Res. 2012; 95:138–146. [PubMed: 22266753]
5. Joutel A, Andreux F, Gaulis S, et al. The ectodomain of the Notch3 receptor accumulates within the cerebrovasculature of CADASIL patients. J Clin Invest. 2000; 105:597–605. [PubMed: 10712431]
6. Monet-Leprêtre M, Haddad I, Baron-Menguy C, et al. Abnormal recruitment of extracellular matrix proteins by excess Notch3 ECD: a new pathomechanism in CADASIL. Brain. 2013; 136:1830–1845. [PubMed: 23649698]
7. Yamamoto Y, Craggs LJL, Watanabe A, et al. Brain microvascular accumulation and distribution of the NOTCH3 ectodomain and granular osmiophilic material in CADASIL. J Neuropathol Exp Neurol. 2013; 72:416–431. [PubMed: 23584202]
8. Kast J, Hanecker P, Beaufort N, et al. Sequestration of latent TGF-β binding protein 1 into CADASIL-related Notch3-ECD deposits. Acta Neuropathol Commun. 2014; 2:96. [PubMed: 25190493]
9. Joutel A, Haddad I, Ratelade J, Nelson MT. Perturbations of the cerebrovascular matrisome: a convergent mechanism in small vessel disease of the brain? J Cereb Blood Flow Metab. 2015 Apr 8. Epub ahead of print. doi: 10.1038/jcbfm.2015.62
10. Brew K, Nagase H. The tissue inhibitors of metalloproteinases (TIMPs): an ancient family with structural and functional diversity. Biochim Biophys Acta. 2010; 1803:55–71. [PubMed: 20080133]
11. Preissner KT, Reuning U. Vitronectin in vascular context: facets of a multitalented matricellular protein. Semin Thromb Hemost. 2011; 37:408–424. [PubMed: 21805447]
12. Joutel A, Monet-Lepretre M, Gosele C, et al. Cerebrovascular dysfunction and microcirculation rarefaction precede white matter lesions in a mouse genetic model of cerebral ischemic small vessel disease. J Clin Invest. 2010; 120:433–445. [PubMed: 20071773]
13. Janssen A, Hoellenriegel J, Fogarasi M, et al. Abnormal vessel formation in the choroid of mice lacking tissue inhibitor of metalloprotease-3. Invest Ophthalmol Vis Sci. 2008; 49:2812–2822. [PubMed: 18408187]
14. Zheng X, Saunders TL, Camper SA, et al. Vitronectin is not essential for normal mammalian development and fertility. Proc Natl Acad Sci U S A. 1995; 92:12426–12430. [PubMed: 8618914]
15. Cognat E, Baron-Menguy C, Domenga-Denier V, et al. Archetypal Arg169Cys mutation in NOTCH3 does not drive the pathogenesis in cerebral autosomal dominant arteriopathy with subcortical infarcts and leucoencephalopathy via a loss-of-function mechanism. Stroke. 2014; 45:842–849. [PubMed: 24425116]
16. Capone C, Faraco G, Peterson JR, et al. Central cardiovascular circuits contribute to the neurovascular dysfunction in angiotensin II hypertension. J Neurosci. 2012; 32:4878–4886. [PubMed: 22492044]
17. Girouard H, Park L, Anrather J, et al. Angiotensin II attenuates endothelium-dependent responses in the cerebral microcirculation through nox-2-derived radicals. Arterioscler Thromb Vasc Biol. 2006; 26:826–832. [PubMed: 16439707]
18. Niwa K, Kazama K, Younkin L, et al. Cerebrovascular autoregulation is profoundly impaired in mice overexpressing amyloid precursor protein. Am J Physiol Heart Circ Physiol. 2002; 283:H315–H323. [PubMed: 12063304]
19. Cognat E, Cleophax S, Domenga-Denier V, Joutel A. Early white matter changes in CADASIL: evidence of segmental intramyelinic oedema in a pre-clinical mouse model. Acta Neuropathol Commun. 2014; 2:49. [PubMed: 24886907]

20. Basu R, Fan D, Kandalam V, et al. Loss of Timp3 gene leads to abdominal aortic aneurysm formation in response to angiotensin II. J Biol Chem. 2012; 287:44083–44096. [PubMed: 23144462]
21. Basu R, Lee J, Morton JS, et al. TIMP3 is the primary TIMP to regulate agonist-induced vascular remodelling and hypertension. Cardiovasc Res. 2013; 98:360–371. [PubMed: 23524300]
22. Iadecola C, Nedergaard M. Glial regulation of the cerebral microvasculature. Nat Neurosci. 2007; 10:1369–1376. [PubMed: 17965657]
23. Dabertrand F, Krøigaard C, Bonev AD, et al. Potassium channelopathy-like defect underlies early-stage cerebrovascular dysfunction in a genetic model of small vessel disease. Proc Natl Acad Sci U S A. 2015; 112:E796–E805. [PubMed: 25646445]
24. Cipolla, MJ. The cerebral circulation. 1st. San Rafael, CA: Morgan & Claypool Life Sciences; 2009.
25. Joutel A. Pathogenesis of CADASIL: transgenic and knock-out mice to probe function and dysfunction of the mutated gene, Notch3, in the cerebrovasculature. Bioessays. 2011; 33:73–80. [PubMed: 20967782]
26. Arboleda-Velasquez JF, Manent J, Lee JH, et al. Hypomorphic Notch 3 alleles link Notch signaling to ischemic cerebral small-vessel disease. Proc Natl Acad Sci U S A. 2011; 108:E128–E135. [PubMed: 21555590]
27. Olzscha H, Schermann SM, Woerner AC, et al. Amyloid-like aggregates sequester numerous metastable proteins with essential cellular functions. Cell. 2011; 144:67–78. [PubMed: 21215370]
28. Kim S, Nollen EAA, Kitagawa K, et al. Polyglutamine protein aggregates are dynamic. Nat Cell Biol. 2002; 4:826–831. [PubMed: 12360295]
29. Hall CN, Reynell C, Gesslein B, et al. Capillary pericytes regulate cerebral blood flow in health and disease. Nature. 2014; 508:55–60. [PubMed: 24670647]
30. Dunn KM, Nelson MT. Neurovascular signaling in the brain and the pathological consequences of hypertension. Am J Physiol Heart Circ Physiol. 2014; 306:H1–H14. [PubMed: 24163077]
31. Hill RA, Tong L, Yuan P, et al. Regional blood flow in the normal and ischemic brain is controlled by arteriolar smooth muscle cell contractility and not by capillary pericytes. Neuron. 2015; 87:95–110. [PubMed: 26119027]
32. Blobel CP. ADAMs: key components in EGFR signalling and development. Nat Rev Mol Cell Biol. 2005; 6:32–43. [PubMed: 15688065]
33. Iadecola C. The pathobiology of vascular dementia. Neuron. 2013; 80:844–866. [PubMed: 24267647]
34. Daneman R, Zhou L, Agalliu D, et al. The mouse blood-brain barrier transcriptome: a new resource for understanding the development and function of brain endothelial cells. PloS One. 2010; 5:e13741. [PubMed: 21060791]
35. Zhang Y, Chen K, Sloan SA, et al. An RNA-sequencing transcriptome and splicing database of glia, neurons, and vascular cells of the cerebral cortex. J Neurosci. 2014; 34:11929–11947. [PubMed: 25186741]

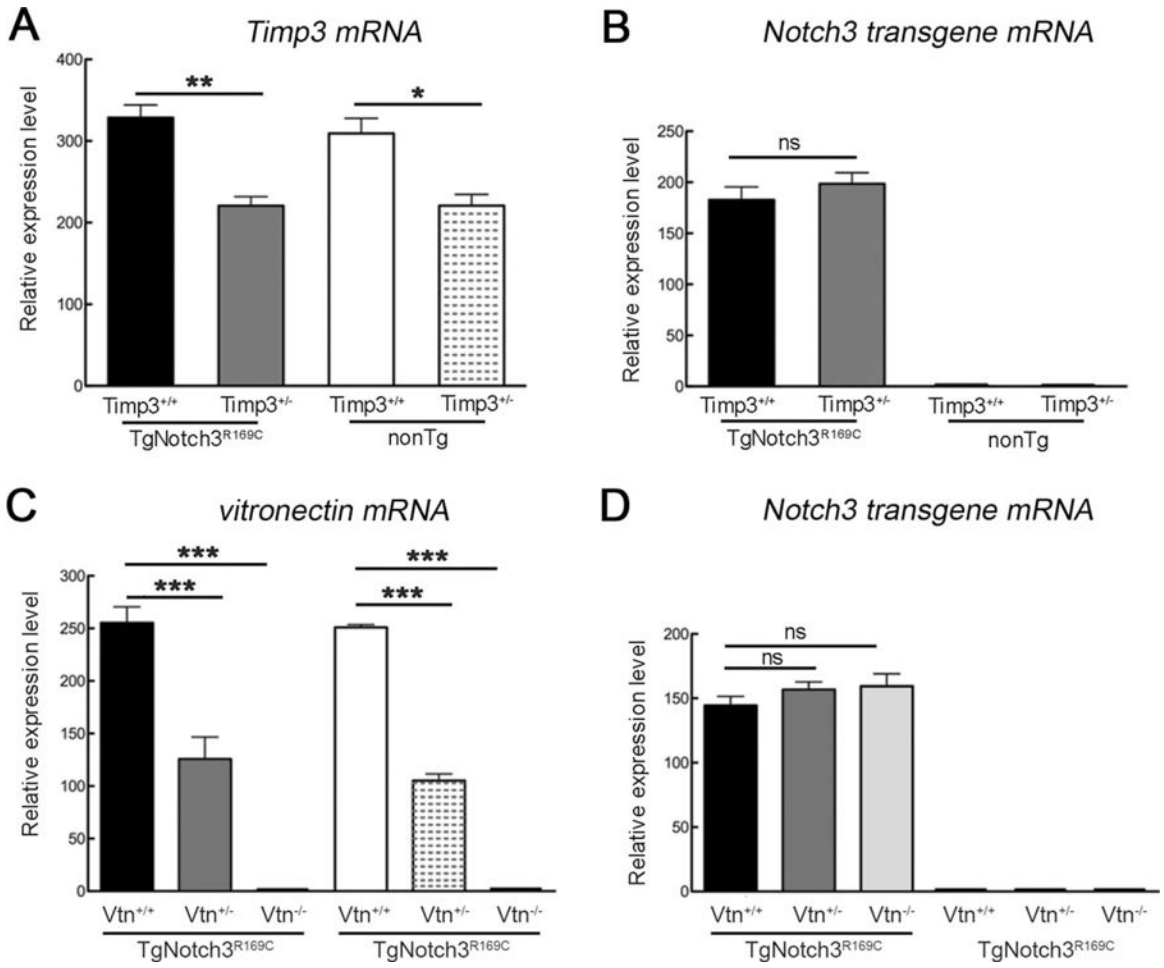

FIGURE 1.

Genetic reduction of *Timp3* or *vitronectin* in *TgNotch3*^{R169C} mice does not affect *Notch3* transgene mRNA expression. Expression levels of *Timp3* (A), rat *Notch3* transgene (B, D), and *vitronectin* (C) mRNA were analyzed by quantitative reverse transcription polymerase chain reaction in brain arteries from 6-month-old *TgNotch3*^{R169C}*;Timp3*$^{+/+}$, *TgNotch3*^{R169C}*;Timp3*$^{+/-}$, and control nontransgenic (*nonTg*) littermate mice (A, B), and *TgNotch3*^{R169C}*;Vtn*$^{+/+}$, *TgNotch3*^{R169C}*;Vtn*$^{+/-}$, *TgNotch3R*^{169C}*;Vtn*$^{-/-}$, and control *nonTg* littermate mice (C, D). Target mRNA levels were normalized to those of β-actin (n = 4–8 samples per genotype). Significance was determined by 1-way analysis of variance followed by Tukey post hoc test (*$p < 0.05$, **$p < 0.01$, ***$p < 0.001$). ns = nonsignificant.

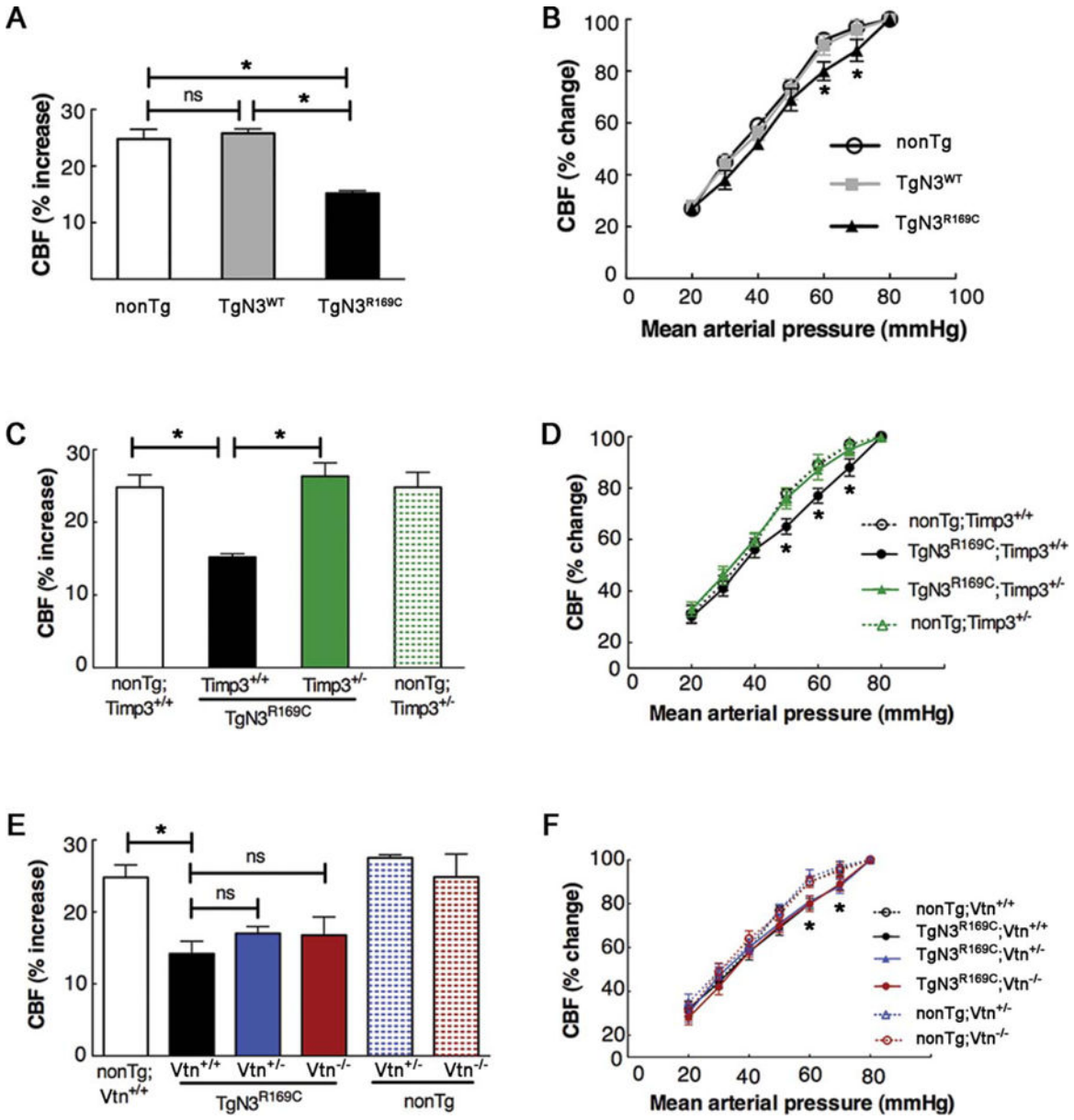

FIGURE 2.

Timp3 haploinsufficiency protects against attenuated functional hyperemia and altered cerebral blood flow (CBF) autoregulation in *TgNotch3*^{R169C} mice, whereas genetic reduction or ablation of *vitronectin* has no effect. CBF changes evoked by whisker stimulation (functional hyperemia; A, C, E) and controlled mean arterial pressure (MAP) reduction (B, D, F) were assessed in various 6-month-old transgenic mouse models (n = 5–8 males per genotype). (A, B) Single transgenic *TgNotch3*^{R169C} (*TgN3*^{R169C}) and *TgNotch3*^{WT} (*TgN3*^{WT}) mice, and nontransgenic (*nonTg*) littermate controls. (C, D) Double-mutant *TgN3*^{R169C}*; Timp3*$^{+/-}$ mice, with *Timp3* haploinsufficiency in the context of *Notch3*^{R169C} overexpression; *nonTg;Timp3*$^{+/+}$*, nonTg;Timp3*$^{+/-}$, and *TgNotch3*^{R169C}*;Timp3*$^{+/+}$ mice were included as controls. (E, F) Double-mutant *TgN3*^{R169C}*;Vtn*$^{+/-}$ and *TgN3*^{R169C}*;Vtn*$^{-/-}$ mice, with *vitronectin* haploinsufficiency and

complete ablation, respectively, in the context of *Notch3*^{R169C} overexpression; *nonTg;Vtn*$^{+/+}$, *nonTg;Vtn*$^{+/-}$, *nonTg;Vtn*$^{-/-}$, *and TgNotch3*^{R169C}*;Vtn*$^{+/+}$ mice were included as controls. Functional hyperemia was strongly attenuated in *TgN3*^{R169C} mice compared to *TgN3*^{WT} and *nonTg* littermate mice, and *TgN3*^{R169C} mice showed an impaired relationship between CBF and MAP; CBF was significantly different between *TgN3*^{R169C} and *TgN3*^{WT} or *nonTg* mice at MAP values of 60 to 70mmHg. CBF responses were similarly impaired in *TgN3*^{R169C} mice expressing wild-type *Timp3* (*TgN3*^{R169C}*;Timp3*$^{+/+}$) or wild-type *vitronectin* (*TgN3*^{R169C}*;Vtn*$^{+/+}$), whereas these responses were not altered in *nonTg* littermate mice with or without genetic reduction of *Timp3* (*nonTg;Timp3*$^{+/-}$) or *vitronectin* (*nonTg;Vtn*$^{-/-}$). Importantly, *TgN3*^{R169C}*;Timp3*$^{+/-}$ mice exhibited normalized CBF responses to whisker stimulation and a restored relationship between MAP and CBF comparable to that of their *nonTg;Timp3*$^{+/-}$ and *nonTg;Timp3*$^{+/+}$ littermates (C, D). In contrast, neither *TgN3*^{R169C}*;Vtn*$^{+/-}$ nor *TgN3*^{R169C}*;Vtn*$^{-/-}$ mice (E, F) exhibited improved CBF responses. (A, C, E) One-way analysis of variance (ANOVA) followed by Tukey post hoc test; (B, D, F) 2-way repeated measures ANOVA followed by Bonferroni post hoc test (*$p < 0.05$). The main physiological variables for all mice are presented in the Table. ns = nonsignificant.

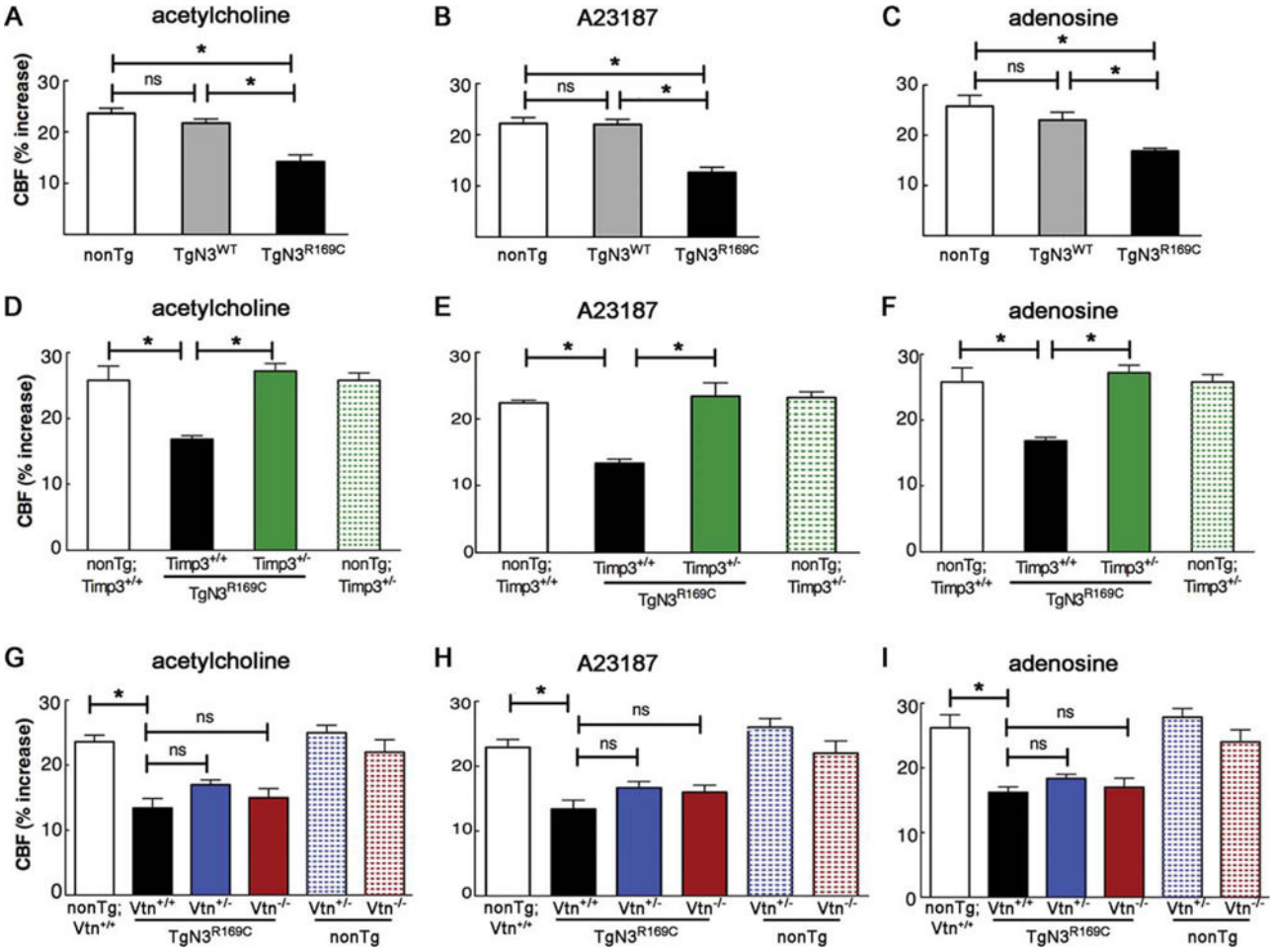

FIGURE 3.

Cerebral blood flow (CBF) responses evoked by endothelium-dependent and endothelium-independent vasodilators are normalized in *TgNotch3*^{R169C} mice by genetic reduction of *Timp3*, but not *vitronectin*. CBF increases evoked by the endothelium-dependent vasodilators acetylcholine (A, D, G) or calcium ionophore A23187 (B, E, H) and smooth muscle–dependent vasodilator adenosine (C, F, I) were analyzed in various 6-month-old transgenic mouse models (n = 5–8 males per genotype). (A–C) Single transgenic *TgNotch3*^{R169C} (*TgN3*^{R169C}) and *TgNotch3*^{WT} (*TgN3*^{WT}) mice, and nontransgenic (*nonTg*) littermate controls. (D–F) Double-mutant *TgN3*^{R169C}*;Timp3*$^{+/-}$ mice, with Timp3 haploinsufficiency in the context of *Notch3*^{R169C} overexpression; *nonTg;Timp3*$^{+/+}$, *nonTg;Timp3*$^{+/-}$, and *TgNotch3*^{R169C}*;Timp3*$^{+/+}$ mice were included as controls. (G–I) Double-mutant *TgN3*^{R169C}*;Vtn*$^{+/-}$ and *TgN3*^{R169C}*;Vtn*$^{-/-}$ mice, with *vitronectin* haploinsufficiency and complete ablation, respectively, in the context of *Notch3*^{R169C} overexpression; *nonTg;Vtn*$^{+/+}$, *nonTg;Vtn*$^{+/-}$, *nonTg;Vtn*$^{-/-}$, *and TgNotch3*^{R169C}*;Vtn*$^{+/+}$ mice were included as controls. All CBF responses were significantly attenuated in *TgN3*^{R169C} mice with wild-type *Timp3* and *vitronectin* (*TgN3*^{R169C}, *TgN3*^{R169C}*;Timp3*$^{+/+}$, *TgN3*^{R169C}*;Vtn*$^{+/+}$). Responses of *TgN3*^{R169C}*;Vtn*$^{+/-}$ and *TgN3*^{R169C}*;Vtn*$^{-/-}$ mice were similarly impaired, whereas *TgN3*^{R169C}*;Timp3*$^{+/-}$ mice had normal responses that were comparable to those of *nonTg;Timp3*$^{+/+}$ and *nonTg;Timp3*$^{+/-}$ littermates. Significance was

determined by 1-way analysis of variance followed by Tukey post hoc test ($*p < 0.05$). The main physiological variables for all mice are presented in the Table. ns = nonsignificant.

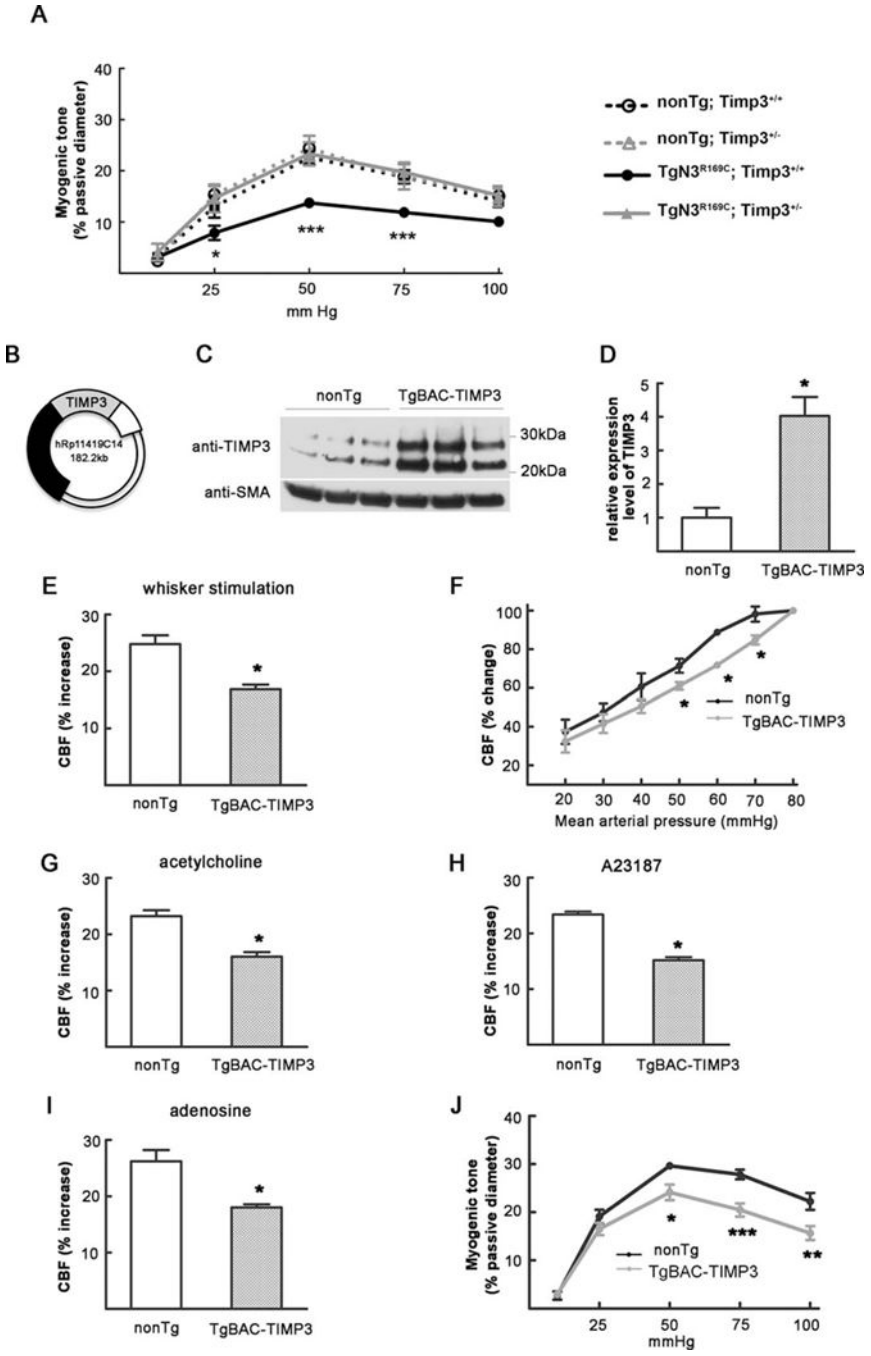

FIGURE 4.

Timp3 haploinsufficiency protects against reduced myogenic tone in *TgNotch3*^{R169C} mice and *TIMP3* overexpression reproduces the cerebrovascular deficits of *TgNotch3*^{R169C} mice. (A) Myogenic responses are normal in nontransgenic (*non-Tg*);*Timp3*$^{+/-}$ mice, are attenuated in *TgN3*^{R169C};*Timp3*$^{+/+}$ mice, and are normalized in *TgN3*^{R169C};*Timp3*$^{+/-}$ mice (n = 7–8 mice per genotype). (B) Schematic representation of the bacterial artificial chromosome (BAC) containing the human *TIMP3* locus. (C, D) Immunoblot analysis of brain arteries (C) shows approximately a 4-fold increase in TIMP3 levels in *TgBAC-TIMP3*

mice compared with *nonTg* littermates (D; n = 3 samples per group, each prepared with brain arteries dissected from 2 mice). (E–I) Cerebral blood flow (CBF) changes evoked by whisker stimulation (E), the endothelium-dependent vasodilators acetylcholine (G) or calcium ionophore A23187 (H), and smooth muscle–dependent vasodilator adenosine (I) are strongly reduced in 6-month-old *TgBAC-TIMP3* mice (n = 5–6 mice per genotype). (F) *TgBAC-TIMP3* mice show an impaired relationship between CBF and mean arterial pressure (MAP). CBF is statistically different between *TgBAC-TIMP3* and *nonTg* at MAP values of 50 to 70mmHg. The main physiological variables for all mice are presented in the Table. (J) Myogenic responses are attenuated in *TgBAC-TIMP3* mice compared with *nonTg* littermates (n = 7–8 per genotype). Significance was determined by Student *t* test (D, E, G–I) or 2-way repeated measures analysis of variance followed by Bonferroni post hoc test (A, F, J; $*p < 0.05$, $**p < 0.01$, $***p < 0.001$). SMA = smooth muscle actin.

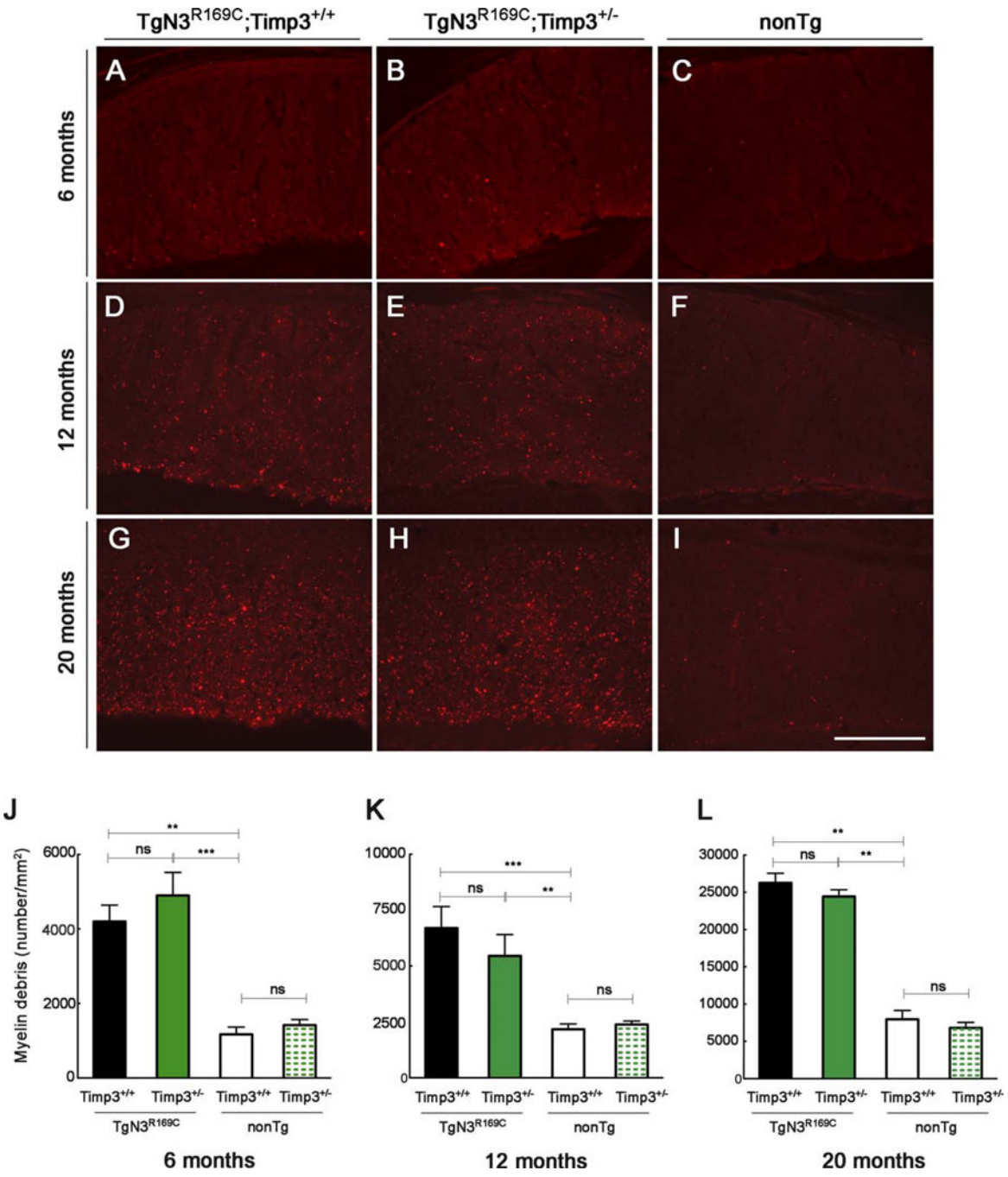

FIGURE 5.

Genetic reduction of *Timp3* does not ameliorate white matter lesions in *TgNotch3*^{R169C} mice. (A–I) Representative images of immunostaining for myelin basic protein (SMI94 antibody) in the corpus callosum (genu) from *TgN3*^{R169C}*;Timp3*$^{+/+}$, *TgN3*^{R169C}*;Timp3*$^{+/-}$, and control nontransgenic (*nonTg*) littermates at (A–C) 6 months of age, (D–F) 12 months of age, and (G–I) 20 months of age. (J–L) Myelin debris spots per square millimeter of corpus callosum were quantified at 6 months of age (J; n = 5–10 mice), 12 months of age (K; n = 4–7 mice), and 20 months of age (L; n = 5–9 mice). Significance was determined by

1-way analysis of variance followed by Bonferroni post hoc test (* *$p < 0.01$, ***$p < 0.001$). Scale bar = 140 μm. ns = nonsignificant.

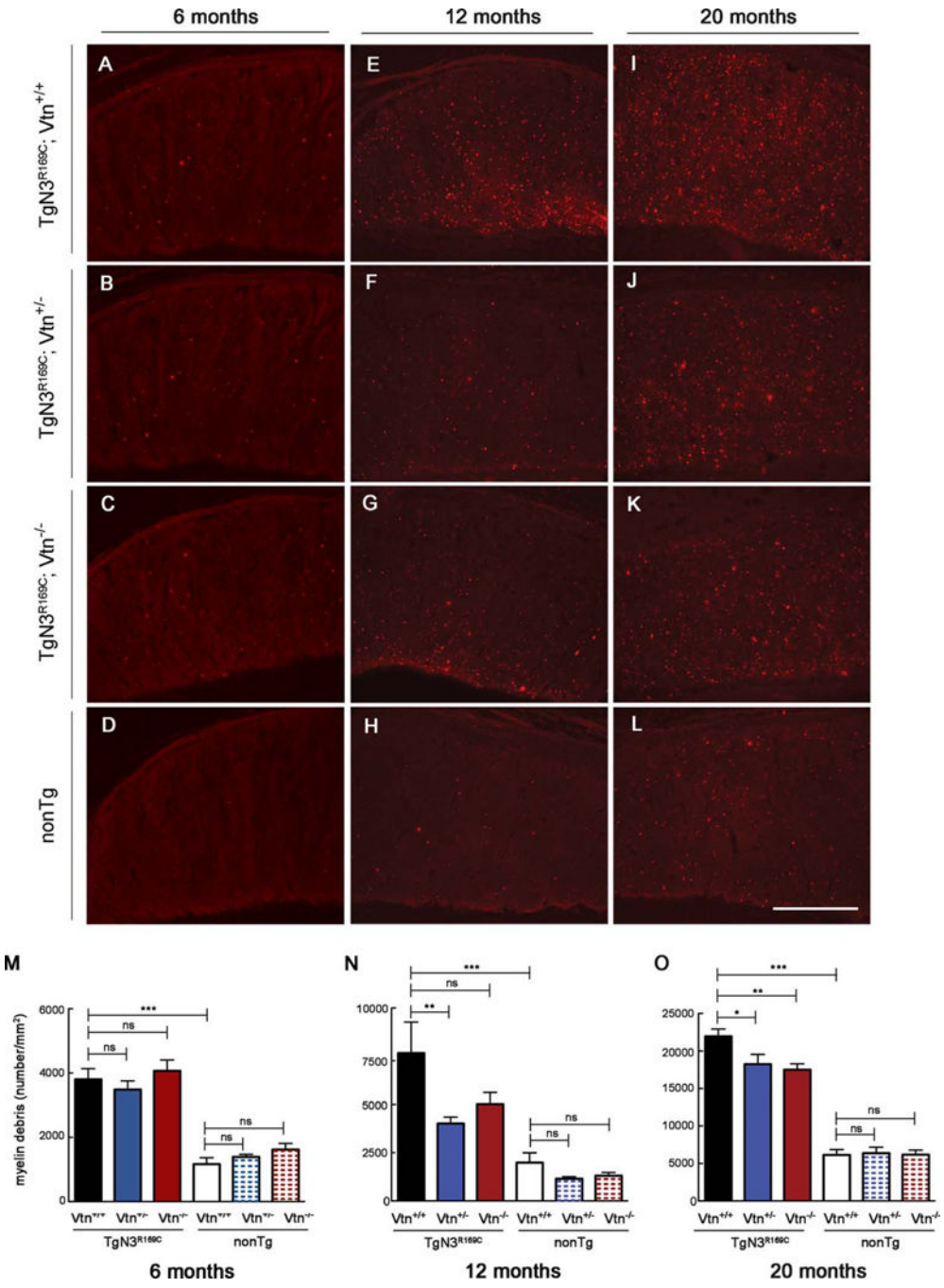

FIGURE 6.

Genetic reduction of *vitronectin* decreases the number of white matter lesions in *TgNotch3*^{R169C} mice. Representative images show immunostaining for myelin basic protein (SMI94 antibody) in the corpus callosum (genu) from *TgN3*^{R169C}*;Vtn*$^{+/+}$, *TgN3*^{R169C}*;Vtn*$^{+/-}$, *TgN3*^{R169C}*;Vtn*$^{-/-}$, and control nontransgenic (*nonTg*) littermates at (A–D) 6 months of age, (E–H) 12 months of age, and (I–L) 20 months of age. (M–O) Quantification of myelin debris spots per square millimeter of corpus callosum shows comparable amount of debris in *TgN3*^{R169C}*;Vtn*$^{+/+}$, *TgN3*^{R169C}*;Vtn*$^{+/-}$, and

TgN3^{R169C};*Vtn*$^{-/-}$ at 6 months (M; n = 5–9 mice) but significantly less debris in *TgN3*^{R169C};*Vtn*$^{+/-}$ mice and a trend toward less debris in *TgN3*^{R169C};*Vtn*$^{-/-}$ mice compared with age-matched *TgN3*^{R169C};*Vtn*$^{+/+}$ mice at 12 months (N; n = 6–9 mice). Both *TgN3*^{R169C};*Vtn*$^{+/-}$ and *TgN3*^{R169C};*Vtn*$^{-/-}$ mice have significantly fewer debris spots than age-matched *TgN3*^{R169C};*Vtn*$^{+/+}$ mice at 20 months of age (O; n = 7–10 mice). Significance was determined by 1-way analysis of variance followed by Bonferroni post hoc test (*p < 0.05, **p < 0.01, ***p < 0.001). Scale bar = 140 μm. ns = nonsignificant.

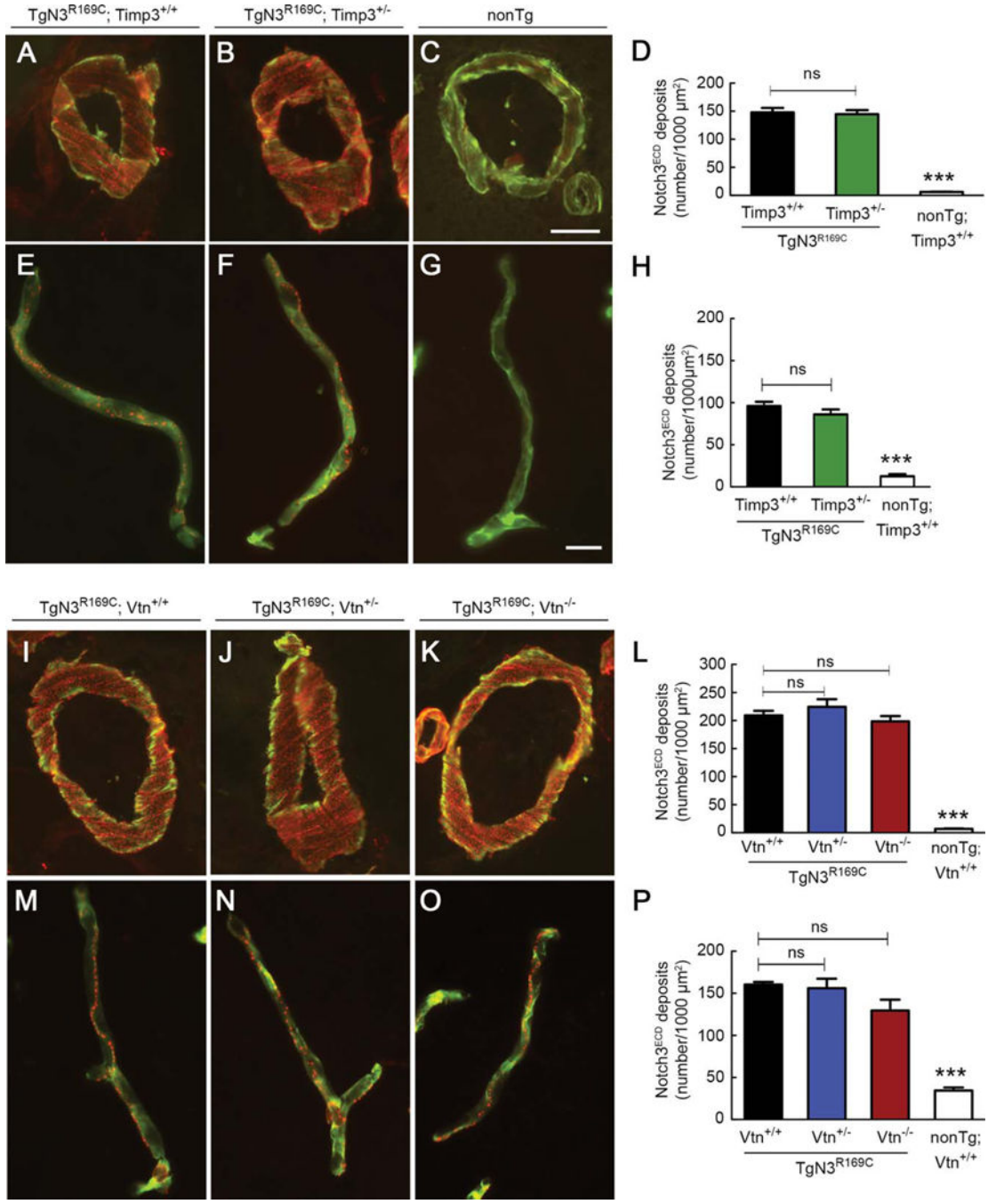

FIGURE 7.

Notch3^{ECD} deposition in brain vessels is unaffected by genetic reduction of *Timp3* or *vitronectin*. Notch3^{ECD} deposits were quantified in brain arteries and capillaries from mice with the indicated genotypes at 6 months of age (A–H) and 12 months of age (I–P). Representative images show brain arteries coimmunostained with anti-Notch3^{ECD} antibody (red) and fluorescein isothiocyanate–conjugated anti–smooth muscle a-actin antibody (green; A–C, I–K) and brain capillaries coimmunostained with anti-Notch3^{ECD} antibody (red) and antiperlecan antibody (green; E–G, M–0). Quantification of Notch3^{ECD} deposit

numbers per 1,000 μm^2 in brain arteries (D, L) and brain capillaries (H, P) shows a significantly higher number of deposits in transgenic mice compared to nontransgenic (*nonTg*) mice, but a comparable number of deposits in *TgN3*^{R169C} mice with normal or reduced expression of *Timp3* (D, H) and normal, reduced, or no expression of *vitronectin* (L, P; n = 4–5 mice per genotype). Significance was determined by 1-way analysis of variance followed by Bonferroni post hoc test (***$p < 0.001$). Scale bars = 10 μm (A–C, I–K) and 15 μm (E–G, M–0). ns = nonsignificant.

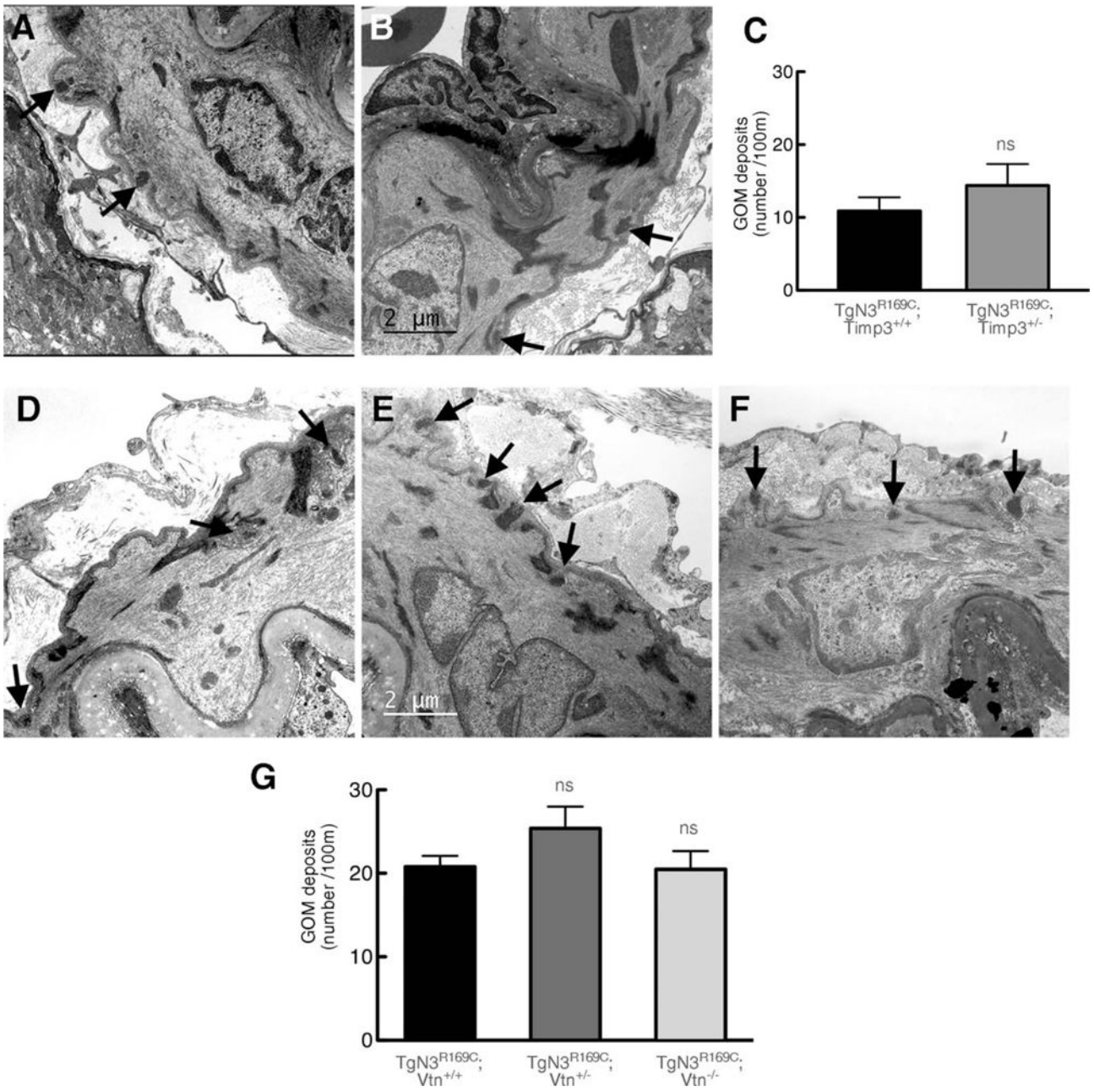

FIGURE 8.

Genetic reduction of *Timp3* or *vitronectin* does not affect the number of granular osmiophilic material (GOM) deposits. Shown are representative electron micrographs of segments of middle cerebral artery from $TgN3^{R169C};Timp3^{+/+}$ (A) and $TgN3^{R169C};Timp3^{+/-}$ mice (B) aged 6 months, and from $TgN3^{R169C};Vtn^{+/+}$ (D), $TgN3^{R169C};Vtn^{+/-}$ (E), and $TgN3^{R169C};Vtn^{-/-}$(F) mice aged 12 months. Arrows point to GOM deposits. (C, G) Quantification shows that the number of GOM deposits is comparable between $TgN3^{R169C};Timp3^{+/+}$ and $TgN3^{R169C};Timp3^{+/-}$ mice (C) and between $TgN3^{R169C};Vtn^{+/+}$, $TgN3^{R169C};Vtn^{+/-}$ and $TgN3^{R169C};Vtn^{-/-}$ mice (G; n = 4 mice per genotype). Significance

was determined by Student *t* test (C) or 1-way analysis of variance followed by Tukey post hoc test (G). Scale bar = 2 μm. ns = nonsignificant.

TABLE

Main Physiological Variables of Mice Studied in Figures 2–4

Genotype (age, mo)	No.	MAP, mmHg	pCO_2, mmHg	pO_2, mmHg	pH
nonTg (6)	6	78 ± 6	34 ± 3	125 ± 5	7.33 ± 0.1
TgNotch3^{R169C} (6)	6	74 ± 2	35 ± 2	126 ± 3	7.34 ± 0.10
TgNotch3^{WT} (6)	5	79 ± 4	36 ± 3	127 ± 4	7.33 ± 0.09
nonTg;Vtn$^{+/+}$ (6)	5	78 ± 4	34 ± 2	126 ± 5	7.33 ± 0.1
TgNotch3^{R169C}*;Vtn*$^{+/+}$ (6)	5	75 ± 3	35 ± 1	125 ± 7	7.34 ± 0.01
nonTg;Vtn$^{+/-}$ (6)	6	76 ± 2	35 ± 2	127 ± 6	7.34 ± 0.02
TgNotch3^{R169C}*;Vtn*$^{+/-}$ (6)	6	74 ± 2	35 ± 2	127 ± 5	7.35 ± 0.02
nonTg;Vtn$^{-/-}$ (6)	7	75 ± 6	34 ± 1	127 ± 3	7.34 ± 0.02
TgNotch3^{R169C}*;Vtn*$^{-/-}$ (6)	8	76 ± 4	35 ± 2	125 ± 6	7.35 ± 0.02
nonTg;Vtn$^{+/+}$ (12)	5	72 ± 4	35 ± 1	123 ± 4	7.35 ± 0.1
TgNotch3^{R169C}*;Vtn*$^{+/+}$ (12)	7	76 ± 2	34 ± 2	126 ± 4	7.34 ± 0.01
nonTg;Vtn$^{+/-}$ (12)	7	76 ± 2	35 ± 2	125 ± 5	7.34 ± 0.02
TgNotch3^{R169C}*;Vtn*$^{+/-}$ (12)	6	79 ± 4	36 ± 2	126 ± 5	7.33 ± 0.1
nonTg;Timp3$^{+/+}$ (6)	6	79 ± 3	37 ± 2	124 ± 4	7.34 ± 0.08
TgNotch3^{R169C}*;Timp3*$^{+/+}$ (6)	6	77 ± 2	37 ± 3	126 ± 5	7.34 ± 0.15
nonTg;Timp3$^{+/-}$ (6)	5	75 ± 5	36 ± 2	125 ± 4	7.32 ± 0.1
TgNotch3^{R169C}*;Timp3*$^{+/-}$ (6)	6	74 ± 6	36 ± 3	127 ± 5	7.33 ± 0.07
nonTg (6)	5	79 ± 3	34 ± 2	126 ± 5	7.32 ± 0.1
TgBAC-TIMP3 (6)	5	90 ± 3[a]	37 ± 2	128 ± 4	7.33 ± 0.1

All mice used in these studies are males.

[a] $p < 0.05$ versus nontransgenic (*nonTg*), 1-way analysis of variance followed by Tukey post hoc test.

MAP = mean arterial pressure.